ACS APPLIED MATERIALS & INTERFACES

Research Article

www.acsami.org

Regenerable Fluorescent Nanosensors for Monitoring and Recovering Metal Ions Based on Photoactivatable Monolayer Self-Assembly and Host–Guest Interactions

Wei Wang,[†,‡] Nai-Kei Wong,[‡] Mingda Sun,[†] Chunqiu Yan,[†] Siyuan Ma,[‡] Qingbiao Yang,*[,†] and Yaoxian Li[†]

[†]Department of Chemistry, Jilin University, Changchun 130021, China

[‡]Department of Chemistry, The University of Hong Kong, Hong Kong, China

Supporting Information

ABSTRACT: Efficient detection, removal, and recovery of heavy metal ions from aqueous environments represents a technologically challenging and ecologically urgent question in the face of increasing metal-related pollution and poisoning across the globe. Although small-molecule and entrapment-based nanoparticle sensors have been extensively explored for metal detection, neither of these extant strategies satisfies the critical needs for high-performance sensors that are inexpensive, efficient, and recyclable. Here we first report the development of a regenerable fluorescent nanosensor system for the selective and sensitive detection of multiple heavy metal ions, based on light-switchable monolayer self-assembly and host–guest interactions. The system exploits photocontrolled inclusion and exclusion responses of an α-cyclodextrin (CD)-containing surface conjugated with photoisomerizable azobenzene as a supramolecular system that undergoes reversible assembly and disassembly. The metal nanosensors can be facilely fabricated and photochemically switched between three chemically distinct entities, each having an excellent capacity for selective detecting specific metal ions (namely, Cu^{2+}, Fe^{3+}, Hg^{2+}) in a chemical system and in assays on actual water samples with interfering contaminants.

KEYWORDS: *photochemistry, monolayer self-assembly, metal nanosensor, fluorescence, supramolecular materials*

INTRODUCTION

In recent decades, anthropogenic impact on heavy metal distribution in the environment has been magnified by expanding world population and overconsumption, with alarming ramifications such as metal poisoning, accelerated air/soil/water pollution, and general diminishment of human health.[1−5] At the same time, efficient detection, removal, and recovery of heavy metal ions from aqueous environments represents a technologically challenging and ecologically urgent question. Current strategies for metal detection have been largely based on small-molecule sensors that have limited reusability and applicability only in the homogeneous (aqueous) phase.[6−8] To tackle these shortages, considerable efforts have been made to develop metal nanosensors as an alternative, though such nanoparticle-based probes also have their share of limitations such as poor synthesis reproducibility, high costs, low sensitivity, and rigid assay requirements.[9−11] Thus, far, composite nanosensors[9,12−14] based on physical entrapunent of probe in a solid matrix have been extensively explored for metal detection, but this strategy is nonideal for precise metal detection due to the nanoparticles' intrinsic inhomogeneity, inconsistency in specific surface area, uneven analyte permeability, and tendency for fluorophore leaching in aqueous samples.[15,16] For metal detection apt for environmental applications, it is critical to develop high-performance sensors that are inexpensive, efficient, and recyclable.

To our best knowledge, there have been no reports on nanosensors that can be photochemically switched and recycled for detection or harvest of different analytes. As light is an external stimulus capable of transducing a chemical change with minimal invasiveness,[17−21] we envisioned that a light-controlled nanosensor system can be a promising approach to metal ion detection. Factors such as ease of availability and manipulation, coupled with rapid photochemical reaction rates and low photoinduced byproducts, make light-controlled systems[21−27] practically ideal.

Among photoisomerizable switches, azobenzene is one of the most widely employed because of its high sensitivity in reversible trans- and cis-photoisomerization upon UV and visible light irradiation, respectively.[28−30] It is thus regarded as a powerful molecular switch with a broad range of applications. Accordingly, based on the well-defined photoinduced behavior of azobenzene, various azobenzene-containing stimuli-responsive self-assembling systems have been synthesized, which has a wide application scope that includes drug delivery,[28] template synthesis,[29] switchable catalysts,[31] and liquid crystals.[32] In particular, the "host–guest" supramolecular systems based on α-cyclodextrin (α-CD)-azobenzene have received intense attention in recent years for their utility as nanostructured

Received: February 16, 2015
Accepted: April 7, 2015
Published: April 7, 2015

DOI: 10.1021/acsami.5b01509
ACS Appl. Mater. Interfaces 2015, 7, 8868−8875

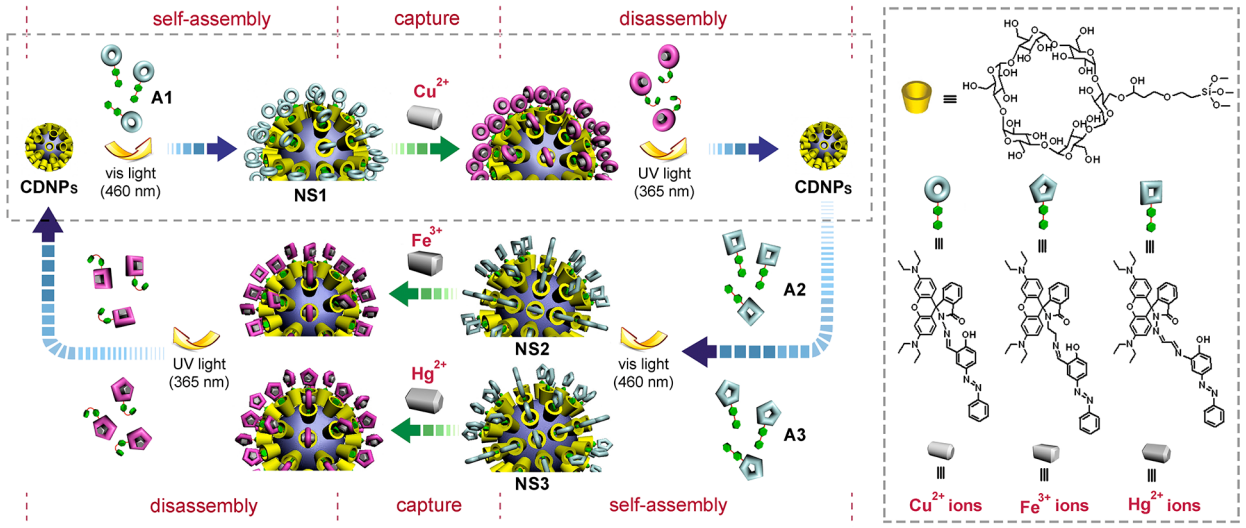

Figure 1. Chemical structures and schematic illustration of the preparation of **NS1**, **NS2**, and **NS3** fluorescent sensors for different metal ions.

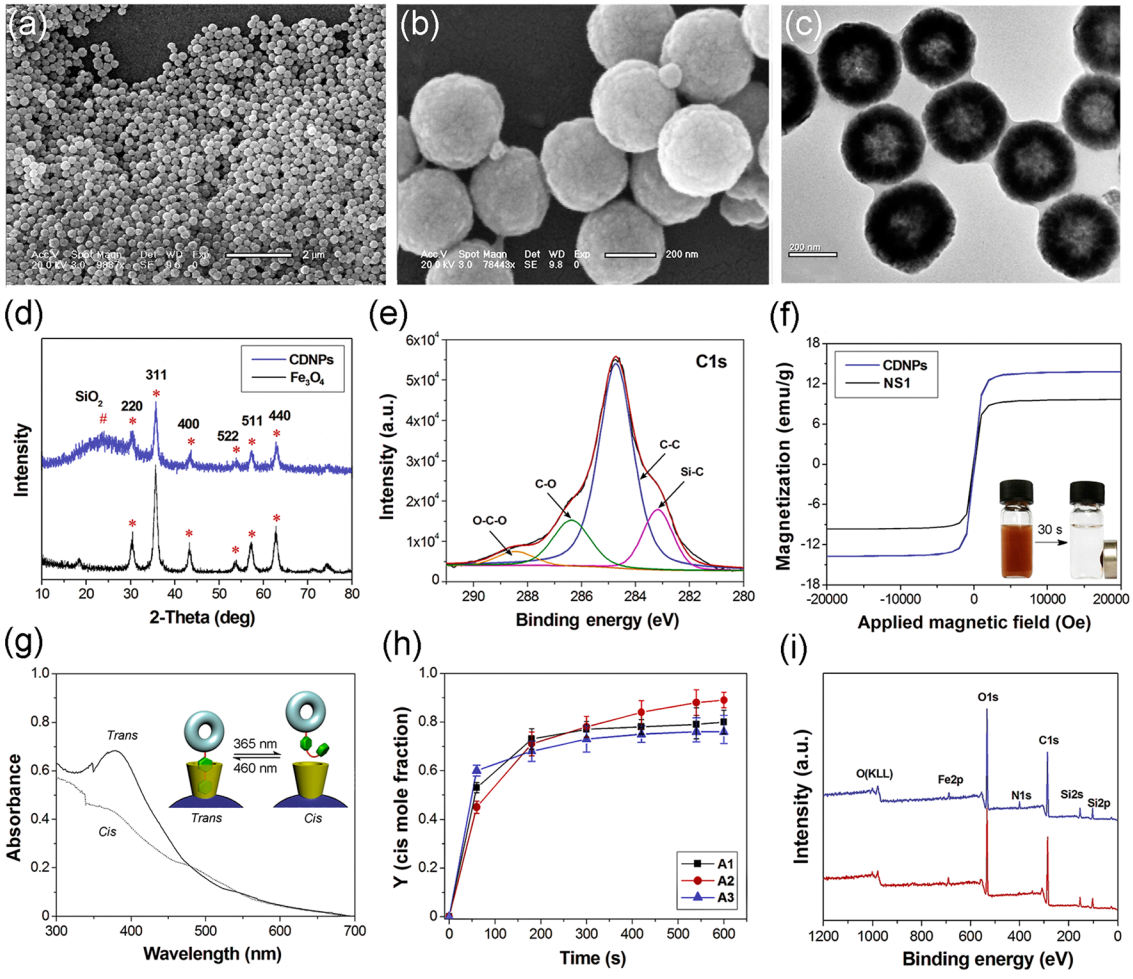

Figure 2. SEM images of **NS1** (a) and (b). (c) TEM images of nanosensor **NS1**. (d) The XRD patterns of the CDNPs (blue line) and Fe_3O_4 nanoparticles (black line). (e) High-resolution XPS spectrum of C 1s of the CDNPs nanoparticles (colored lines represent the deconvolution curves). (f) The magnetic hysteresis loops of **NS1** (blue line) and CDNPs (black line); inset: photographs of an aqueous suspension of **NS1** (left) and after magnetic capture within 30 s (right). (g) Change in UV−vis absorption spectra for S1 after photoirradiation by UV light (at 365 nm). (h) Kinetics graph of **NS1**, **NS2**, and **NS3** showing photoisomerization from trans to cis with respect to time (in seconds). (i) XPS survey spectra of the **NS1** nanoparticles before (blue tracing) and after (red tracing) UV irradiation with rinsing with DMF solution.

functional materials[33−36] and molecular devices.[37−42] In host−guest inclusion complexation involving α-CD/azobenzene, the *trans* isomer of azobenzene can be well included by α-CD with a high association constant (2.8×10^4 mol L^{-1}) in aqueous

DOI: 10.1021/acsami.5b01509
ACS Appl. Mater. Interfaces 2015, 7, 8868−8875

solution.[29,43] cis−trans isomerization of the azo group by UV−visible light can be exploited to control the inclusion and exclusion of azobenzene units, which is accompanied by significant changes in its molecular dipole moment and absorption spectrum.

Here we present a new strategy for developing fluorescent nanoparticles with light-switchable abilities for detection of multiple heavy metal ions. We attempted to make use of photocontrolled inclusion and exclusion responses of an α-CD-containing surface conjugated with azobenzene as a rechargeable supramolecular system that can undergo reversible assembly and disassembly (Figure 1). This proposed metal nanosensor system, modified with a photoactive switchable monolayer, can be photochemically switched between three chemically distinct entities, each having an excellent capacity for selective detection of specific metal ions (namely, Cu^{2+}, Fe^{3+}, Hg^{2+}). A major advantage of this method is that it allows self-assembly of guest (organic fluorescent sensor units) and host (α-CD) molecules on the surface of nanomaterials (silicon base), in which a guest molecule could be optimally positioned and oriented in the detection system to function efficiently, with minimal interference to host surface properties. We believe that this work illustrates a model system that successfully combines photochemistry and host−guest supramolecular chemistry for developing photochemically switchable nanosensors, functional enhancement of sensing nanomaterials, as well as application of heavy metal ion detection.

First, the α-CD-functionalized magnetic nanoparticles (denoted as CDNPs) (host) was prepared, as described in previous reports with slight modification.[44,45] To realize the photocontrolled assembly and disassembly, we designed and synthesized three functionalized rhodamine-based azobenzene derivatives as guest molecules (denoted as **A1**−**A3**). Then, the inclusion complex nanosensors (**NS1**, **NS2**, and **NS3**) were easily prepared from CDNPs and azobenzene-containing guest molecules (**A1**−**A3**) by a "self-assembly" technique as reported in our previous work[46] (Figure 1). Detailed procedures for synthesizing host/guest molecules can be found in the Supporting Information.

RESULTS AND DISCUSSION

It has been suggested that small nanoparticle (NP) size and high specific surface area are associated with greater contact of analyte with the surface of a nanosensor, which is conducive to probe sensitivity.[47] Previously, we have successfully developed a strategy for synthesizing hollow-core ferromagnetic NPs,[46] with small NP size and high specific surface area. In this work, the sizes and shapes of the CDNPs were evaluated by scanning electron microscopy (SEM) and transmission electron microscopy (TEM). SEM imaging showed that the CDNPs nanostructures were uniformly sized, with a smooth surface and an average diameter of about 250 nm (Figure 2a,b). TEM images confirmed that the microspheres (NPs) possessed hollow structures in the range of 70−90 nm in diameter and about 90 nm the thickness of the shell (Figure 2c). XRD patterns of the synthesized Fe_3O_4 and CDNPs displayed several relatively strong reflection peaks in the 2θ region of 10−80°. Six discernible diffraction peaks in Figure 2d can be indexed to (220), (311), (400), (422), (511), and (440), which match well with the database information about magnetite in JCPDS (JCPDS Card, 19-629) file and a broad featureless X-ray diffraction (XRD) peak at low diffraction angle, which corresponds to the amorphous SiO_2 shell. This result suggests that the Fe_3O_4 nanoparticles were successfully coated onto the SiO_2 shell. In XPS, the high-resolution C 1s spectrum broadly corresponds to four peak components, as calculated by XPS Peak Fit (software), with binding energies of about 283.17, 285.00, 286.45, and 288.66 eV (Figure 2e), attributable to C−Si, C−C, C−O, and O−C−O species, respectively.[45,46,48,49] As the O−C−O peak is characteristic of α-CD, the result confirms that modification of the NP with α-CD was successful.

It should be noted in Figure 2f that CDNPs and **NS1** samples have low coercivity and no obvious hysteresis, which indicates that the nanosensors have superparamagnetism.[50] The saturation magnetization (Ms) values for CDNPs and **NS1** were 13.25 and 8.92 emu/g, respectively, suggesting that the **NS1** inherited strongly magnetic properties from Fe_3O_4 nanoparticles. Thus, magnetic separation ability of **NS1** in this detection method can also offer a simple and efficient route to isolate and concentrate target toxic metal ions from various environments.

As expected, the azobenzene part at the tail of the functionalized nanoparticle can be photoinduced to become isomerized in trans (entry) or cis (egress) configurations. In UV−vis absorption spectra, photoisomerization of the azobenzene-functionalized nanoparticles was observed in an aprotic solvent, *N*,*N*-dimethyllformamide (DMF), at a concentration of 0.5 g/L (Figure 2g). Before irradiation with UV light, the observed spectrum for the cis isomer was typical of azobenzene derivatives, while the more stable trans isomer was characterized by a strong $\pi-\pi^*$ transition at 349 nm, which agrees well with previous reports.[51] Upon UV irradiation at 365 nm, the absorption band at around 349 nm decreases remarkably, indicating that reverse photoisomerization of **A1** from the trans to cis isomer configuration.[52] Owing to the photoinduced structural change from a rod-like trans configuration to a hook-like cis configuration, the cavity of the α-CD host cannot host the bulky cis isomer of the azo group. As a result of such spatial mismatch between the host and guest, **A1** was forced to be detached from the surface of the nanoparticles.[28,53] After 10 min of UV irradiation, further significant changes in the spectra were not detected, indicating the existence of a photostationary state containing about 76% cis isomer of **NS1** (Figure 2h). The fraction of cis isomers in the photostationary state was calculated from absorbance at λ_{max} (349 nm) for the $\pi-\pi^*$ absorption of the trans isomer at time t according to the following equation:[52,54,55]

$$Y = [\text{cis}]_t/[\text{trans}]_0 = (1 - A/A_0)/(1 - \varepsilon_{\text{cis}}/\varepsilon_{\text{trans}}) \quad (1)$$

where Y stands for the fraction of cis isomer generated in the medium (DMF), A_0 the initial absorbance for trans isomer only, A the absorbance after each UV irradiation, and $\varepsilon_{\text{cis}}/\varepsilon_{\text{trans}}$ the ratio of molar absorption coefficient for cis and trans isomers. Similarly, the fractions of cis iosmers for **NS2** and **NS3** in the photostationary state were 88% and 72%, respectively. By alternating irradiation of the solution with UV and visible light, the host and guest species can undergo repeated forward and reverse photoisomerization, which thus constitutes a recyclable detection system.

Attachment and detachment of the fluorescent sensor units from CDNPs was confirmed and analyzed by XPS wide-scan spectra and Fourier transform infrared spectroscopy (Figure 2i). To illustrate with **NS1** as an example, the peak at 399.4 eV was contributed by the N═N of azobenzene group,[56−58] and the rate of integral area of the peak was 76.0%, from which we calculated that the nitrogen content of azobenzene to be 3.42%,

DOI: 10.1021/acsami.5b01509
ACS Appl. Mater. Interfaces 2015, 7, 8868−8875

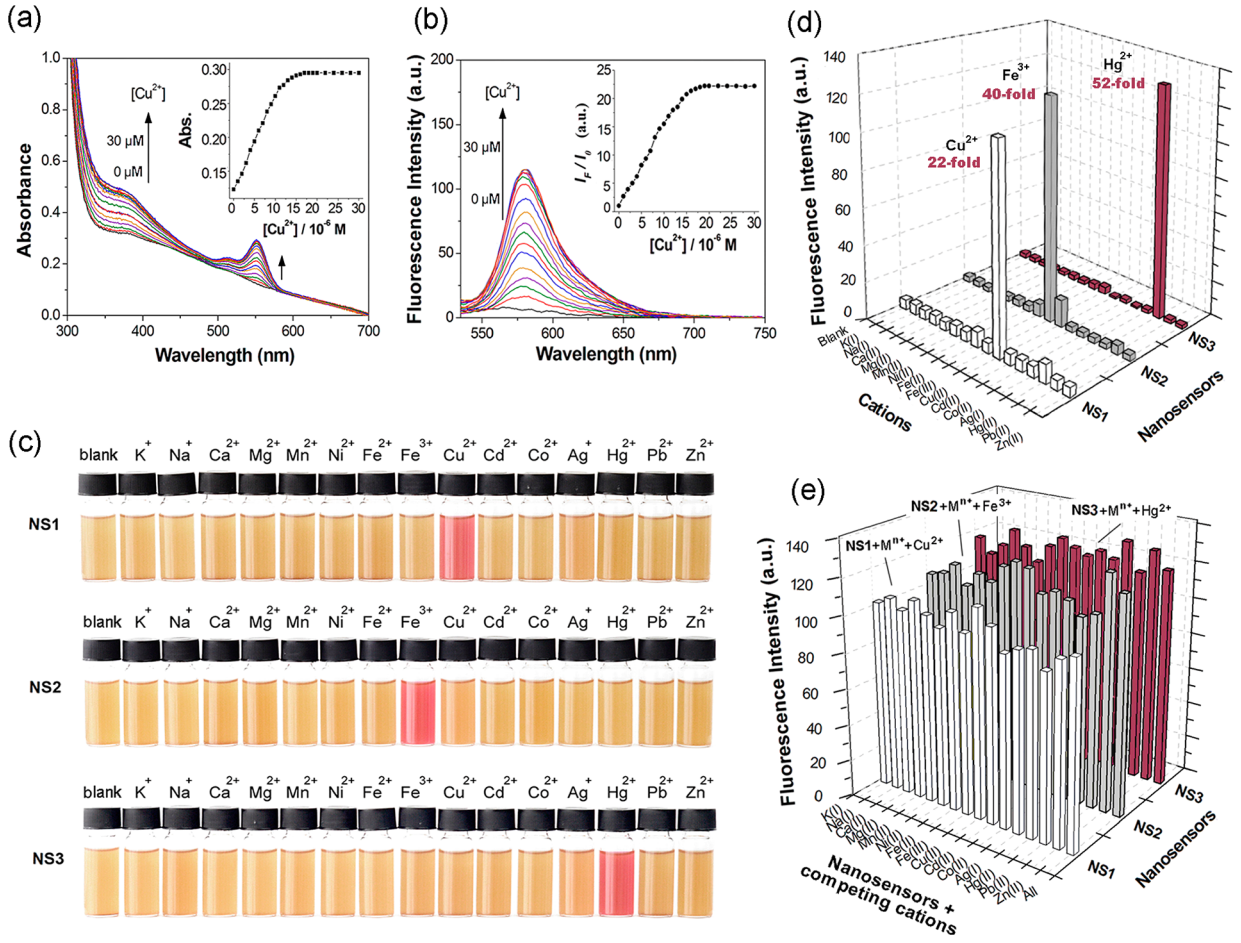

Figure 3. (a) UV−vis spectra of **NS1** in CH_3CN-H_2O in the presence of different amounts of Cu^{2+}; inset shows absorbance intensity as a function of Cu^{2+} concentration. (b) Fluorescent spectra of **S1** in the absence and presence of Cu^{2+} (1.0×10^{-6} to 30×10^{-6} mol L^{-1}); inset shows fluorescence intensity as a function of Cu^{2+} concentration. (c) Photograph of **NS1**, **NS2**, and **NS3** in the presence of various metal ions (1.0×10^{-4} mol L^{-1} except Cu^{2+} is 1.5×10^{-6} mol L^{-1}) in CH_3CN-H_2O solution. (d) Histogram of fluorescence intensity of **NS1**, **NS2**, **NS3** at 578 nm versus increasing concentration of Cu^{2+}, Fe^{3+}, Hg^{2+}. (e) Fluorescence responses of **NS1**, **NS2**, and **NS3** to various metal ions and Cu^{2+}, Fe^{3+}, and Hg^{2+} in the presence of other metal ions in aqueous solution (CH_3CN/H_2O, 1:10, v/v, buffered at pH 7.2 with 20 μM HEPES buffer, excitation was at 500 nm, and emission was monitored at 578 nm).

implying that **A1** was present as a coating on CDNPs. However, when the nanoparticles were irradiated with UV and rinsed with DMF solution, the content of N was reduced to 0.88%, suggesting that nitrogen-containing components were washed off. Furthermore, we compared the IR spectra of **NS1** nanoparticles under the following conditions: (1) before and after UV radiation and (2) after illumination of light at 365 nm and rinsing. As expected, the characteristic peaks of the functional groups of **A1** molecules at 1693 cm^{-1} (C═O) and 1512 cm^{-1} (N═N) disappeared (Figure S1 in the Supporting Information).

Next, we investigated spectroscopic properties of the nanosensors **NS1**, **NS2**, and **NS3** (0.5 g L^{-1} in HEPES-buffered CH_3CN-H_2O (1:10, v/v) at pH 7.2) toward a range of metal ions of physiological or ecological significance: K^+, Na^+, Ca^{2+}, Mg^{2+}, Mn^{2+}, Ni^{2+}, Fe^{2+}, Fe^{3+}, Cu^{2+}, Co^{2+}, Cd^{2+}, Ag^+, Hg^{2+}, Pb^{2+}, and Zn^{2+} in aqueous solution. As expected, the three nanosensors **NS1**, **NS2**, and **NS3** showed excellent selectivity and sensitivity toward their respective analytes Cu^{2+}, Fe^{3+}, Hg^{2+}.

The UV absorption spectra of **NS1** with varying Cu^{2+} ions concentrations were recorded, as shown in Figure 3a. Upon addition of Cu^{2+} ions in **NS1** suspension, the peak around 552 nm was significantly enhanced, suggesting the formation of the ring-opened tautomer of **A1** upon Cu^{2+} ions binding. In this case, **NS1** suspension displayed an observable spectral shift from brown to red (Figure S2 in the Supporting Information). It is also noteworthy that a perceptible color change for Cu^{2+} ions as low as 1.0×10^{-5} mol L^{-1}, but not other metal ions, in this system could be detected by visual inspection (Figure 3c). This interesting feature suggests that **NS1** can serve as a facile, selective "naked-eye" off−on probe for Cu^{2+} ions. These observations indirectly confirmed that the fluorescent guest molecules were successfully complexed onto the surface of host supports.

To test the sensitivity of the nanosensor **NS1**, titration of a concentation gradient of Cu^{2+} ions was carried out against a solution of **NS1** (0.5 g L^{-1}) in HEPES-buffered CH_3CN-H_2O (1:10, v/v) at pH 7.2. Upon addition of increasing concentrations of Cu^{2+} ions, the characteristic fluorescence of rhodamine B fluorophore (at 578 nm) was significantly enhanced in a Cu^{2+} concentration-dependent manner (Figure 3b). Kinetically, the nanosensor turned on very rapidly in response to even very low Cu^{2+} concentrations (e.g., 1.0×10^{-6} mol L^{-1}), reaching a fluorescence plateau in about 60 s (Figure S3 in the Supporting Information). Maximum fluorescence

DOI: 10.1021/acsami.5b01509
ACS Appl. Mater. Interfaces 2015, 7, 8868−8875

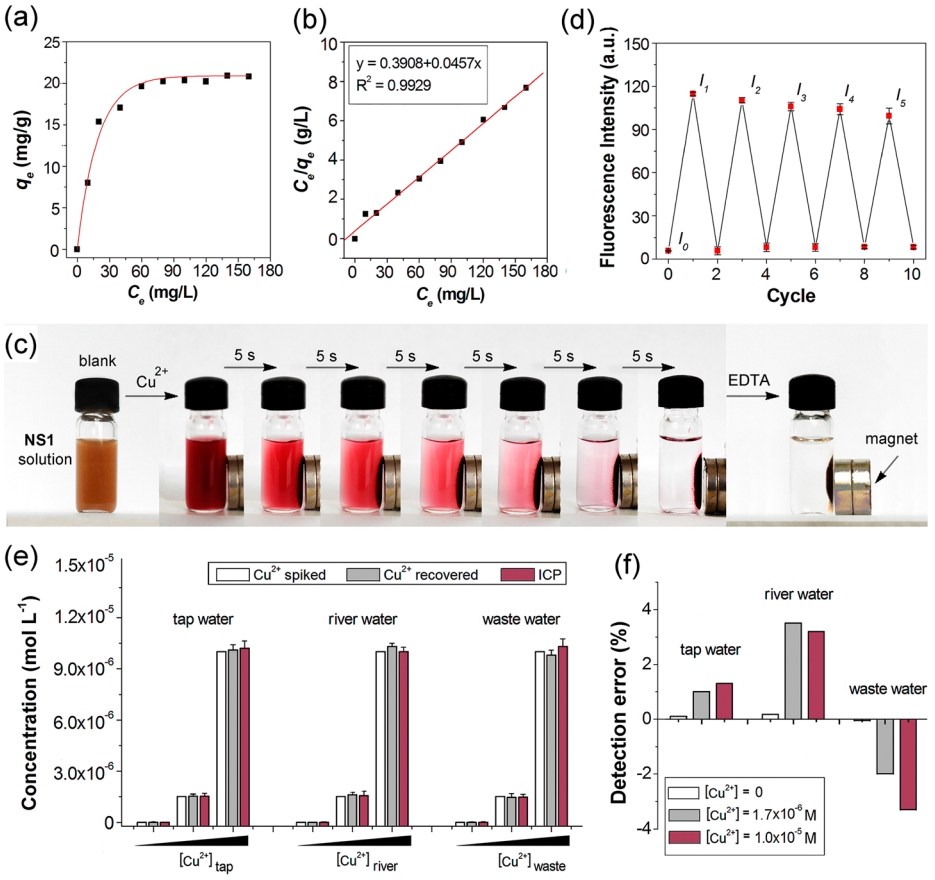

Figure 4. (a) Adsorption isotherm and (b) Langmuir plot of Cu^{2+} on the **NS1**. (c) Dynamic process of separation−concentration of Cu^{2+}-containing **NS1** in the presence of a magnet. (d) Fluorescence response of **NS1** (0.5 g L^{-1}) in the 5×10^{-4} M of Cu^{2+} ions over five complex/stripping cycles, I_0 corresponds to the emission intensity of **NS1**, I_1−I_5 corresponds to the emission of **NS1** with fresh Cu^{2+} ions solutions, respectively. (Excitation was at 500 nm, emission was monitored at 553 nm.) (e) Determination of Cu^{2+} with **NS1** in real samples at the optimum conditions and the detection error for three replicates analysis (f).

intensity was achieved at >2.0×10^{-5} mol L^{-1} Cu^{2+} ions. In addition, a linear relationship was observed between the fluorescence intensity of **NS1** and concentration of Cu^{2+} within the range (1.0×10^{-6})−(1.4×10^{-5}) mol L^{-1} (Figure S4 in the Supporting Information), with a correlation coefficient R^2 = 0.9956. The detection limit, based on the definition by IUPAC (CDL = 3 Sb/m, where Sb is the standard deviation of background fluorescence and m the slope of the calibration curve),[59] was 1.50×10^{-6} mol L^{-1}. This threshold value is much lower than the acceptable value mandated by the EPA (United States Environmental Protection Agency) for the concentration of copper in drinking water (1.5 ppm). Upon the addition of Cu^{2+} ions, there was an obvious fluorescence off−on change of **NS1** at different pH values (shown in Figure S5 in the Supporting Information). And the pH-control emission measurements reveal that **NS1** could respond to Cu^{2+} ions in a pH range from 7 to 12 with little changes of the fluorescent intensity, suggesting that the **NS1** facilitates the quantification of the concentration of Cu^{2+} ions in aqueous solution in a wide pH range. In consideration of most samples analysis of metal ions being neutral, in this study, the medium for metal ions detection was buffered at pH 7.2. The other two nanosensors **NS2** and **NS3** also showed highly comparable levels of sensitivity (Figure S6 in the Supporting Information), with detection limits of 5.92×10^{-7} mol $L^{-1}$and 4.15×10^{-7} mol L^{-1}, respectively. We thus confirmed that our nanosensors possess excellent sensitivity, which can potentially be applied to detect of inorganic $Cu^{2+}/Fe^{3+}/Hg^{2+}$ in biological, pharmaceutical, and ecological samples.

To evaluate the selectivity of **NS1** as a fuorescent nanosensor for Cu^{2+} ions, the fuorescence response of **NS1** upon addition of various biologically and environmentally relevant metal ions (white bars in Figure 3d) was determined. Potentially inteferring ions including K^+, Na^+, Ca^{2+}, Mg^{2+}, Mn^{2+}, Ni^{2+}, Cd^{2+}, Co^{2+}, Pb^{2+}, Zn^{2+}, Hg^{2+}, and Fe^{3+} were tested at 1.0×10^{-4} mol L^{-1}, while the target analyte Cu^{2+} was tested at 1.5×10^{-6} mol L^{-1}. As expected, except for Cu^{2+}, the above-mentioned metal ions produced no or negligible changes in fuorescence intensity as reported by **NS1**. In the prescence of Cu^{2+}, dramatic fluorescence enhancement (>22-fold) relative to blank control was observed, while excess competing Hg^{2+} or Fe^{3+} (1.0×10^{-4} mol L^{-1}) ions only increased the fluorescence response slightly by 1.9 and 2.4-fold, respectively. Similarly, the other two nanosensor **NS2** and **NS3** detected Fe^{3+} (gray bars in Figure 3d) and Hg^{2+} (red bars in Figure 3d) in a highly selective and sensitive manner. In order to further assess any interference from other metal ions in the detection of Cu^{2+} ions, competition experiments were performed in which the fluorescent probe **NS1** was added to a solution of Cu^{2+} ions (1.5×10^{-6} mol L^{-1}) in the presence of excess amounts of other metal ions (1.0×10^{-4} mol L^{-1}) as shown in Figure 2e. The results indicate that these ions had no obvious interference in the detection of Cu^{2+} ions and that **NS1** is a promising selective adsorbent for the separation of Cu^{2+} ions in a mixture

DOI: 10.1021/acsami.5b01509
ACS Appl. Mater. Interfaces 2015, 7, 8868−8875

of metal ions. The other two nanosensors (**NS2** and **NS3**) similarly showed high selectivity and sensitivity toward their corresponding substrates (Fe^{3+} and Hg^{2+}, respectively). Nearly no color and changes in fluorescent intensity were observed in both absorption and emission spectra with interfering metal ions (see gray bars and red bars in Figure 3e).

Almost all current flourescent sensors are capable of only detecting metal ions but not removing or isolating target ions from solutions. In this work, we endowed **NS1** with adsorptive and separative properties to remove Cu^{2+} ions from aqueous solutions. Adsorption equilibrium data of Cu^{2+} ions were analyzed with Langmuir adsorption equation isotherm models (Figure 4a). **NS1** as a monolayered nanosensor was found to possess excellent adsorption capacity for Cu^{2+}, as suggested by high adsorption density (q_e) values (Figure 4b). The maximum adsorption density (q_m) was 22.79 mg of Cu^{2+} ions per gram of **NS1** (0.5 g L^{-1}) (Table S1 in the Supporting Information). Interestingly, as a sorbent, **NS1** was also found to be able to adsorb relatively large amounts of other metal ions (such as Pb^{2+}, Cd^{2+}) whose ionic radius match with the cavity of α-CD in aqueous solutions[60] (see adsorption capacity of **NS1** in Figure S7 in the Supporting Information).

Reversibility of chemosensors is a very important chemical aspect in practical applications. We tested **NS1** (0.5 g L^{-1}) reversibility by alternately exposing it to aqueous Cu^{2+} ion (1.0×10^{-4} mol L^{-1}) solution and aqueous EDTA (5.0×10^{-4} mol L^{-1}) solution and measuring the corresponding fluorescence emission and adsorption density of **NS1**. Our results suggest that emission of **NS1** could be restored. As shown in Figure 4c, **NS1** were able to efficiently capture Cu^{2+} for at least 5 cycles, with a very small decrease in fluorescence intensity (I_5/I_1 = 87.45%) after repeated stripping and wash steps. In contrast, the emission could not be restored when **NS1** was bathed with pure water (negative control for EDTA) even with protracted incubation of >24. In addition, the color of **NS1** also exhibits reversibility upon being alternately treated with Cu^{2+} ions and EDTA (Figure 4d). Figure S8 in the Supporting Information summarizes desorption efficiency for the five sorption−desorption cycles. As shown in Figure S8 in the Supporting Information, the desorption efficiency of Cu^{2+} ions also there did not significantly decrease as the **NS1** regeneration cycles progressed, which indicates that EDTA solution can effectively desorb the Cu^{2+} adsorbed by nanosensors. These results indicated that there was no appreciable loss in adsorption density of the nanosensor over the studied five cycles, it was expected this regeneration capacity indicates that nanosensors could be efficiently reused, and it would be a promising adsorbent for fast removal of metal ions from practical water pollution accidents by heavy metals.

To further assess the applicability of the nanosensors in practical settings, we tested their performance in detecting metal ions in river, tap, or wastewater samples (Figure 4e and Figure S9 in the Supporting Information), which mimic aqueous environments with heighened interferences. We adopted the standard addition method[61,62] and spiked the samples with different amounts of specific metal ions (Cu^{2+}, Fe^{3+}, Hg^{2+}). Each sample was analyzed in four replicates. For confirmation, the metal ion contents were checked with an inductively coupled plasma mass spectrometer (ICP-MS). As summarized in Figure 4e, the results show that the sensor **NS1** is remarkably robust in determining metal ion concentrations in the samples with very high precision and accuracy (Figure 4f). The proposed method is thus suitable for efficient determination of metal ions in such different aqueous samples of complex composition.

CONCLUSIONS

In summary, we reported a fluorescent nanosensor system for the accurate detection of heavy metal ions, which can be facilely fabricated. On the basis of photochemically switchable "host−guest" self-assembly/disassembly, the nanosensors showed excellent selectivity and sensitivity toward different target metal ions. These nanosensors feature rapid turn-on response, "naked-eye" recognition, and high adsorption capacity and can be efficiently recycled and robustly applied to detect trace amounts of analytes in actual water samples. We believe that this strategy provides a promising alternative for developing high-performance sensing materials for the detection, removal, and recovery of heavy metal ions in aqueous solutions. This work should help motivate further exploration of urgently needed nanomaterials capable of addressing metal-related environmental problems.

EXPERIMENTAL SECTION

Materials. Rhodamine B (RhB) and α-cyclodextrin (α-CD) were purchased from Sigma-Aldrich. Hydrazine hydrate (80%), ethylenediamine, glyoxal (40%), and triethylamine were obtained from Alfa. Aniline, salicylaldehyde, and 2-aminophenol were obtained from Aladdin. γ-(2,3-Epoxypropoxy) propytrimethoxysilane (KH-560, 99%) was obtained from Acros Organics. All reagents and inorganic metal salts analytical grade (Shanghai Chemical Reagents Co. China) were used without further purification. The solutions of metal ions were prepared by dissolving salts of NaCl, KCl, $CaCl_2$, $MgSO_4$, $FeCl_3$, $Mn(NO_3)_2{\cdot}6H_2O$, $CoCl_2{\cdot}6H_2O$, $NiCl_2{\cdot}6H_2O$, $Zn(NO_3)_2$, $CdCl_2$, $CuCl_2{\cdot}2H_2O$, $HgCl_2$, $AgNO_3$, and $Pb(NO_3)_2$ in deionized water. Aqueous HEPES-NaOH (0.05 mol L^{-1}) solution was used as a buffer to maintain optimal pH (7. 2) and ionic strength of all solutions in experiments.

Synthesis. All compounds and NPs were synthesized according to Schemes S1 and S2 provided in the Supporting Information. For detailed synthetic information and NMR spectra of reaction intermediates **1**−**5** and the guest molecules **A1**−**A3**, see the Supporting Information.

Characterization. ^1H NMR spectra were measured on a Varian Mercury-300BB and Bruker AV-400 spectrometer with chemical shifts reported as parts per million (in $CDCl_3$, with TMS as an internal standard). The pH values of the test solutions were measured with a glass electrode connected to a Mettler-Toledo Instruments DELTA 320 pH meter (Shanghai, China) and adjusted if necessary. The purified nanosensors **NS1**, **NS2**, and **NS3** were characterized by SEM/HR-TEM analysis/imaging, FT-IR spectroscopy, spectroscopy, and UV−vis spectrophotometry. The average size of the NPs as determined by HR-TEM imaging and vesicle analysis. FT-IR spectra of the products were recorded on a PerkinElmer Paragon1000 FT-IR spectrometer. HRMS were collected with an Agilent1290-micrOTOF Q II (Bruker) spectrometer. Absorption and luminescence spectra were studied on a Shimadzu UV 2100 PC UV−visible spectrophotometer and a Hitachi F-4500 luminescence spectrometer, respectively.

ASSOCIATED CONTENT

Supporting Information

Details regarding experimental procedures and characterization; kinetics of adsorption of Cu^{2+} ions onto **NS1**; FT-IR spectra of **NS1**; response time and sensitivity of nanosensors; standard curves of fluorescence nanosensors versus metal ions; UV−vis and fluorescent spectra of **NS2** and **NS3**; fluorescent measurement of different pH; determination of the metal ions adsorption capacity. This material is available free of charge via the Internet at http://pubs.acs.org.

DOI: 10.1021/acsami.5b01509
ACS Appl. Mater. Interfaces 2015, 7, 8868−8875

AUTHOR INFORMATION

Corresponding Author

*E-mail: yangqb@jlu.edu.cn.

Notes

The authors declare no competing financial interest.

ACKNOWLEDGMENTS

The authors thank the National Natural Science Foundation of China (Grant 21174052) for financial support.

REFERENCES

(1) Nriagu, J. O. A History of Global Metal Pollution. *Science* **1996**, *272*, 223−230.

(2) World Health Organization (WHO). Health Risks of Heavy Metals from Long-Range Transboundary Air Pollution. *Joint WHO/Convention Task Force on the Health Aspects of Air Pollution, Copenhagen, Denmark*, 2007.

(3) Lamborg, C. H.; Hammerschmidt, C. R.; Bowman, K. L.; Swarr, G. J.; Munson, K. M.; Ohnemus, D. C.; Lam, P. J.; Heimbürger, L.-E.; Rijkenberg, M. J.; Saito, M. A. A Global Ocean Inventory of Anthropogenic Mercury Based on Water Column Measurements. *Nature* **2014**, *512*, 65−68.

(4) Huang, R.-J.; Zhang, Y.; Bozzetti, C.; Ho, K.-F.; Cao, J.-J.; Han, Y.; Daellenbach, K. R.; Slowik, J. G.; Platt, S. M.; Canonaco, F. High Secondary Aerosol Contribution to Particulate Pollution During Haze Events in China. *Nature* **2014**, *514*, 218−222.

(5) Tao, T.; Xin, K. Public health: A Sustainable Plan for China's Drinking Water. *Nature* **2014**, *511*, 527−528.

(6) Carter, K. P.; Young, A. M.; Palmer, A. E. Fluorescent Sensors for Measuring Metal Ions in Living Systems. *Chem. Rev.* **2014**, *114*, 4564−4601.

(7) Domaille, D. W.; Zeng, L.; Chang, C. J. Visualizing Ascorbate-triggered Release of Labile Copper Within Living Cells Using a Ratiometric Fluorescent Sensor. *J. Am. Chem. Soc.* **2010**, *132*, 1194−1195.

(8) Wu, J.-S.; Hwang, I.-C.; Kim, K. S.; Kim, J. S. Rhodamine-based Hg^{2+}-selective Chemodosimeter in Aqueous Solution: Fluorescent OFF−ON. *Org. Lett.* **2007**, *9*, 907−910.

(9) Basabe-Desmonts, L.; Reinhoudt, D. N.; Crego-Calama, M. Design of Fluorescent Materials for Chemical Sensing. *Chem. Soc. Rev.* **2007**, *36*, 993−1017.

(10) Kim, H. N.; Ren, W. X.; Kim, J. S.; Yoon, J. Fluorescent and Colorimetric Sensors for Detection of Lead, Cadmium, and Mercury ions. *Chem. Soc. Rev.* **2012**, *41*, 3210−3244.

(11) Ajayaghosh, A.; Arunkumar, E.; Daub, J. A Highly Specific Ca^{2+}-Ion Sensor: Signaling by Exciton Interaction in a Rigid-Flexible-Rigid Bichromophoric "H" Foldamer. *Angew. Chem., Int. Ed.* **2002**, *41*, 1766−1769.

(12) Wang, X.; Drew, C.; Lee, S.-H.; Senecal, K. J.; Kumar, J.; Samuelson, L. A. Electrospun Nanofibrous Membranes for Highly Sensitive Optical Sensors. *Nano Lett.* **2002**, *2*, 1273−1275.

(13) He, X.; Liu, H.; Li, Y.; Wang, S.; Wang, N.; Xiao, J.; Xu, X.; Zhu, D. Gold Nanoparticle-Based Fluorometric and Colorimetric Sensing of Copper (II) Ions. *Adv. Mater.* **2005**, *17*, 2811−2815.

(14) Lee, J. S.; Han, M. S.; Mirkin, C. A. Colorimetric Detection of Mercuric Ion (Hg^{2+}) in Aqueous Media using DNA-Functionalized Gold Nanoparticles. *Angew. Chem.* **2007**, *119*, 4171−4174.

(15) Du, H.; He, G.; Liu, T.; Ding, L.; Fang, Y. Preparation of Pyrene-functionalized Fluorescent Film with a Benzene Ring in Spacer and Sensitive Detection to Picric Acid in Aqueous phase. *J. Photochem. Photobiol., A* **2011**, *217*, 356−362.

(16) Long, Y.; Chen, H.; Yang, Y.; Wang, H.; Yang, Y.; Li, N.; Li, K.; Pei, J.; Liu, F. Electrospun Nanofibrous Film Doped with a Conjugated Polymer for DNT Fluorescence Sensor. *Macromolecules* **2009**, *42*, 6501−6509.

(17) Ferris, D. P.; Zhao, Y.-L.; Khashab, N. M.; Khatib, H. A.; Stoddart, J. F.; Zink, J. I. Light-operated Mechanized Nanoparticles. *J. Am. Chem. Soc.* **2009**, *131*, 1686−1688.

(18) Mal, N. K.; Fujiwara, M.; Tanaka, Y. Photocontrolled Reversible Release of Guest Molecules from Coumarin-modified Mesoporous silica. *Nature* **2003**, *421*, 350−353.

(19) Koçer, A.; Walko, M.; Meijberg, W.; Feringa, B. L. A Light-actuated Nanovalve Derived from a Channel Protein. *Science* **2005**, *309*, 755−758.

(20) Nguyen, T. D.; Leung, K. F.; Liong, M.; Liu, Y.; Stoddart, J. F.; Zink, J. I. Versatile Supramolecular Nanovalves Reconfigured for Light Activation. *Adv. Funct. Mater.* **2007**, *17*, 2101−2110.

(21) Aznar, E.; Casasús, R.; García-Acosta, B.; Marcos, M. D.; Martínez-Máñez, R.; Sancenón, F.; Soto, J.; Amorós, P. Photochemical and Chemical Two-Channel Control of Functional Nanogated Hybrid Architectures. *Adv. Mater.* **2007**, *19*, 2228−2231.

(22) Horie, M.; Sassa, T.; Hashizume, D.; Suzaki, Y.; Osakada, K.; Wada, T. A crystalline Supramolecular Switch: Controlling the Optical Anisotropy Through the Collective Dynamic Motion of Molecules. *Angew. Chem., Int. Ed.* **2007**, *46*, 4983−4986.

(23) Wurpel, G. W.; Brouwer, A. M.; van Stokkum, I. H.; Farran, A.; Leigh, D. A. Enhanced Hydrogen Bonding Induced by Optical Excitation: Unexpected Subnanosecond Photoinduced Dynamics in A Peptide-based [2] Rotaxane. *J. Am. Chem. Soc.* **2001**, *123*, 11327−11328.

(24) Wu, J.; Leung, K. C. F.; Benítez, D.; Han, J. Y.; Cantrill, S. J.; Fang, L.; Stoddart, J. F. An Acid−Base-Controllable [c2] Daisy Chain. *Angew. Chem., Int. Ed.* **2008**, *47*, 7470−7474.

(25) Yu, Y.; Nakano, M.; Ikeda, T. Photomechanics: Directed Bending of A Polymer Film by Light. *Nature* **2003**, *425*, 145−145.

(26) Keaveney, C. M.; Leigh, D. A. Shuttling Through Anion Recognition. *Angew. Chem., Int. Ed.* **2004**, *43*, 1222−1224.

(27) Ikeda, T.; Mamiya, J. i.; Yu, Y. Photomechanics of Liquid-Crystalline Elastomers and Other Polymers. *Angew. Chem., Int. Ed.* **2007**, *46*, 506−528.

(28) Callari, F.; Petralia, S.; Sortino, S. Highly Photoresponsive Monolayer-protected Gold Clusters by Self-assembly of A Cyclodextrin−azobenzene-derived Supramolecular Complex. *Chem. Commun.* **2006**, 1009−1011.

(29) Wei, J.; Liu, Y.; Chen, J.; Li, Y.; Yue, Q.; Pan, G.; Yu, Y.; Deng, Y.; Zhao, D. Azobenzene-Derived Surfactants as Phototriggered Recyclable Templates for the Synthesis of Ordered Mesoporous Silica Nanospheres. *Adv. Mater.* **2014**, *26*, 1782−1787.

(30) Tamai, N.; Miyasaka, H. Ultrafast Dynamics of Photochromic Systems. *Chem. Rev.* **2000**, *100*, 1875−1890.

(31) Tamesue, S.; Takashima, Y.; Yamaguchi, H.; Shinkai, S.; Harada, A. Photoswitchable Supramolecular Hydrogels Formed by Cyclodextrins and Azobenzene Polymers. *Angew. Chem.* **2010**, *122*, 7623−7626.

(32) Tomatsu, I.; Hashidzume, A.; Harada, A. Contrast Viscosity Changes Upon Photoirradiation for Mixtures of Poly (acrylic acid)-based α-cCyclodextrin and Azobenzene Polymers. *J. Am. Chem. Soc.* **2006**, *128*, 2226−2227.

(33) Ma, X.; Zhao, Y. Biomedical Applications of Supramolecular Systems Based on Host−Guest Interactions. *Chem. Rev.* **2014**, DOI: 10.1021/cr500392w.

(34) Zhang, L.; Chang, H.; Hirata, A.; Wu, H.; Xue, Q.-K.; Chen, M. Nanoporous Gold Based Optical Sensor for Sub-ppt Detection of Mercury Ions. *ACS Nano* **2013**, *7*, 4595−4600.

(35) Peng, L.; You, M.; Wu, C.; Han, D.; Öçsoy, I.; Chen, T.; Chen, Z.; Tan, W. Reversible Phase Transfer of Nanoparticles Based on Photoswitchable Host−Guest Chemistry. *ACS Nano* **2014**, *8*, 2555−2561.

(36) Wang, C.; Wang, Z.; Zhang, X. Superamphiphiles as Building Blocks for Supramolecular Engineering: Towards Functional Materials and Surfaces. *Small* **2011**, *7*, 1379−1383.

(37) Patra, D.; Zhang, H.; Sengupta, S.; Sen, A. Dual Stimuli-Responsive, Rechargeable Micropumps via "Host−Guest" Interactions. *ACS Nano* **2013**, *7*, 7674−7679.

DOI: 10.1021/acsami.5b01509
ACS Appl. Mater. Interfaces 2015, 7, 8868−8875

(38) Kuad, P.; Miyawaki, A.; Takashima, Y.; Yamaguchi, H.; Harada, A. External Stimulus-Responsive Supramolecular Structures Formed by A Stilbene Cyclodextrin Dimer. *J. Am. Chem. Soc.* **2007**, *129*, 12630−12631.
(39) Inoue, Y.; Kuad, P.; Okumura, Y.; Takashima, Y.; Yamaguchi, H.; Harada, A. Thermal and Photochemical Switching of Conformation of Poly (ethylene glycol)-Substituted Cyclodextrin with An Azobenzene Group at the Chain End. *J. Am. Chem. Soc.* **2007**, *129*, 6396−6397.
(40) Nalluri, S. K. M.; Ravoo, B. J. Light-Responsive Molecular Recognition and Adhesion of Vesicles. *Angew. Chem., Int. Ed.* **2010**, *49*, 5371−5374.
(41) Zhao, Q.; Wang, Y.; Yan, Y.; Huang, J. Smart Nano Carrier: Self-Assembly of Bacteria-Like Vesicles with Photo Switchable Cilia. *ACS Nano* **2014**, *8*, 11341−11349.
(42) Lv, C.; Wang, Z.; Wang, P.; Tang, X. Photodegradable Polyurethane Self-Assembled Nanoparticles for Photocontrollable Release. *Langmuir* **2012**, *28*, 9387−9394.
(43) Liu, Z.; Jiang, M. Reversible Aggregation of Gold Nanoparticles Driven by Inclusion Complexation. *J. Mater. Chem.* **2007**, *17*, 4249−4254.
(44) Sun, L.; Li, Y.; Sun, M.; Wang, H.; Xu, S.; Zhang, C.; Yang, Q. Porphyrin-Functionalized Fe_3O_4@SiO_2 Core/Shell Magnetic Colorimetric Material for Detection, Adsorption and Removal of Hg^{2+} in Aqueous Solution. *New J. Chem.* **2011**, *35*, 2697−2704.
(45) Ji, Y.; Liu, X.; Guan, M.; Zhao, C.; Huang, H.; Zhang, H.; Wang, C. Preparation of Functionalized Magnetic Nanoparticulate Sorbents for Rapid Extraction of Biphenolic Pollutants from Environmental Samples. *J. Sep. Sci.* **2009**, *32*, 2139−2145.
(46) Wang, W.; Zhang, Y.; Yang, Q.; Sun, M.; Fei, X.; Song, Y.; Zhang, Y.; Li, Y. Fluorescent and Colorimetric Magnetic Microspheres as Nanosensors for Hg^{2+} in Aqueous Solution Prepared by a Sol−Gel Grafting Reaction and Host−Guest Interaction. *Nanoscale* **2013**, *5*, 4958−4965.
(47) An, K. H.; Jeong, S. Y.; Hwang, H. R.; Lee, Y. H. Enhanced Sensitivity of a Gas Sensor Incorporating Single-Walled Carbon Nanotube−Polypyrrole Nanocomposites. *Adv. Mater.* **2004**, *16*, 1005−1009.
(48) Xu, F.; Zhang, Z.; Ping, Y.; Li, J.; Kang, E.; Neoh, K. Star-Shaped Cationic Polymers by Atom Transfer Radical Polymerization from β-Cyclodextrin Cores for Nonviral Gene Delivery. *Biomacromolecules* **2009**, *10*, 285−293.
(49) Tan, C. J.; Chua, H. G.; Ker, K. H.; Tong, Y. W. Preparation of Bovine Serum Albumin Surface-Imprinted Submicrometer Particles with Magnetic Susceptibility Through Core-Shell Miniemulsion Polymerization. *Anal. Chem.* **2008**, *80*, 683−692.
(50) Tago, T.; Hatsuta, T.; Miyajima, K.; Kishida, M.; Tashiro, S.; Wakabayashi, K. Novel Synthesis of Silica-Coated Ferrite Nanoparticles Prepared using Water-in-Oil Microemulsion. *J. Am. Chem. Soc.* **2002**, *85*, 2188−2194.
(51) Misra, A.; Shahid, M. Chromo and Fluorogenic Properties of Some Azo−Phenol Derivatives and Recognition of Hg^{2+} Ion in Aqueous Medium by Enhanced Fluorescence. *J. Phys. Chem. C* **2010**, *114*, 16726−16739.
(52) Patton, D.; Park, M.-K.; Wang, S.; Advincula, R. C. Evanescent Waveguide and Photochemical Characterization of Azobenzene-Functionalized Dendrimer Ultrathin Films. *Langmuir* **2002**, *18*, 1688−1694.
(53) Li, W.; Wang, Y.; Chen, L.; Huang, Z.; Hu, Q.; Ji, J. Light-Regulated Host−Guest Interaction as A New Strategy for Intracellular PEG-Detachable Polyplexes to Facilitate Nuclear Entry. *Chem. Commun.* **2012**, *48*, 10126−10128.
(54) JoonáKim, J.; HoonáKim, S. Negative Solovatochromism of Azo Dyes Derived from (Dialkylamino) thiazole Dimers. *Chem. Commun.* **2000**, 753−754.
(55) Raymo, F. M.; Cejas, M. A. Supramolecular Association of Dopamine with Immobilized Fluorescent Probes. *Org. Lett.* **2002**, *4*, 3183−3185.
(56) Guo, Z.; Feng, Y.; Zhu, D.; He, S.; Liu, H.; Shi, X.; Sun, J.; Qu, M. Light-Switchable Single-Walled Carbon Nanotubes Based on Host−Guest Chemistry. *Adv. Funct. Mater.* **2013**, *23*, 5010−5018.
(57) Liu, Y.; Yu, Z.-L.; Zhang, Y.-M.; Guo, D.-S.; Liu, Y.-P. Supramolecular Architectures of β-Cyclodextrin-Modified Chitosan and Pyrene Derivatives Mediated by Carbon Nanotubes and Their DNA Condensation. *J. Am. Chem. Soc.* **2008**, *130*, 10431−10439.
(58) Xie, J.; Wang, H.; Bai, H.; Yang, P.; Shi, M.; Guo, P.; Wang, C.; Yang, W.; Song, H. Wormlike Micelle Assisted Rod Coating: A General Method for Facile Fabrication of Large-Area Conductive Nanomaterial Thin Layer onto Flexible Plastics. *ACS Appl. Mater. Interfaces* **2012**, *4*, 2891−2896.
(59) Irving, H.; Freiser, H.; West, T. IUPAC Compendium of Analytical Nomenclature. In *Definitive Rules*; Pergamon Press: Oxford, U.K., 1981.
(60) Norkus, E. Metal Ion Complexes with Native Cyclodextrins. An Overview. *J. Inclusion Phenom. Macrocyclic Chem.* **2009**, *65*, 237−248.
(61) Tessier, A.; Campbell, P. G.; Bisson, M. Sequential Extraction Procedure for the Speciation of Particulate Trace Metals. *Anal. Chem.* **1979**, *51*, 844−851.
(62) Li, Z.; Chang, X.; Zou, X.; Zhu, X.; Nie, R.; Hu, Z.; Li, R. Chemically-Modified Activated Carbon with Ethylenediamine for Selective Solid−Phase Extraction and Preconcentration of Metal Ions. *Anal. Chim. Acta* **2009**, *632*, 272−277.

DOI: 10.1021/acsami.5b01509
ACS Appl. Mater. Interfaces 2015, 7, 8868−8875